RSC Advances

ROYAL SOCIETY OF CHEMISTRY

www.rsc.org/advances

Journal Name

ARTICLE

Luminescence and slow magnetic relaxation of isostructural 2D lanthanide metal-organic frameworks derived from both nicotinate *N*-oxide and glutarate

Received 00th January 20xx,
Accepted 00th January 20xx

DOI: 10.1039/x0xx00000x

www.rsc.org/

Cai-Ming Liu,[a,*] De-Qing Zhang,[a] Xiang Hao,[a] and Dao-Ben Zhu[a]

Three lanthanide coordination polymers containing both nicotinate *N*-oxide and glutarate, $\{[Ln(NNO)(glu)] \cdot 0.25H_2O\}_\infty$ (Ln = Eu, **1**; Ln = Gd, **2**; Ln = Dy, **3**; HNNO = nicotinic acid *N*-oxide, H_2glu = glutaric acid), have been hydrothermally synthesized, which are isostructural, showing 2D layer network structures. The europium(III) species displays typical narrow fluorescent emission bands of the lanthanide ion, with the absolute emission quantum yield of 0.055 and the fluorescence lifetime of 4.2 ns. Magnetic determinations revealed that a weak antiferromagnetic interaction exists in the gadolinium(III) complex, while the dysprosium(III) analogue exhibits field-induced two-step magnetic relaxation, with an effective thermal barrier of 44.2 K

Introduction

Recently, metal–organic frameworks(MOFs) based on trivalent lanthanides, which possess interesting spectroscopic and magnetic properties due to their unique 4*f*-electrons, have been found to exhibit intriguing structure diversity and have potential applications in numerous fields[1] such as catalysis,[2] adsorption,[3] separation,[4] light-emitting,[5] magnetic materials,[6] and sensor materials.[7] It is well-known that most trivalent lanthanide ions may display narrow and characteristic fluorescent emissions thanks to internal 4*f*–4*f* electron transitions. Owing to the weak optical absorption for the forbidden 4*f*–4*f* electron transitions, the direct excitation of the lanthanide ions is not efficient enough. However, the import of suitable organic ligands to be the linkers of MOFs may remarkably improve the light absorption and the energy transfer to the lanthanide ions; such an 'antenna effect' can help the lanthanide metal–organic frameworks (LnMOFs) show luminescent properties effectively.[8] Therefore, the choice of bridging ligand is critical to design and construct the luminescent LnMOFs.

On the other hand, the dysprosium (III) ion, which has a big magnetic moment and significant magnetic anisotropy, may meet the demands of a large spin ground state (*S*) and a negative uniaxial magnetic anisotropy (*D*) for a single-molecule magnet (SMM) or single-ion magnet (SIM), thus becomes a prominent element of the SMMs and the SIMs.[9] The SMMs and the SIMs are characterized by slow magnetic relaxation at low temperature, and can be potentially utilized as the molecular materials of high-density information storage, quantum computer and spintronics.[9,10] Recently, many Dy(III) SMMs and Dy(III) SIMs have been explored,[9] however, it remains a big challenge for the assembly of Dy(III) MOFs showing the SMM behaviours.[11] The obstacle probably lies in that the coordination environment and geometry of the Dy(III) ion in the MOFs are not easy to control.

In a continuation of our interest in the assembly of new LnMOFs[12] and new lanthanide-based SMMs,[13] we recently explored a 3D MOF, which is constructed from a unique dysprosium(III) oxalate layer and a 1-hydro-5-chloro-6-oxopyridine-3-carboxylate ($L1^-$) linker, namely, $\{[Dy_2(L1)_2(OX)_2(H_2O)]\cdot 2H_2O\}_\infty$;[12c] we also synthesized a 2D→2D polyrotaxane dysprosium(III) MOF with 4,4'-sulfonyldibenzoate ($L2^{2-}$) linkers, namely, $[Dy_2(L2)_3(H_2O)_5]_\infty$.[12d] Both complexes exhibit two separate magnetic relaxation processes of the SMM behaviours. We are now particularly interested in the 2D LnMOFs with remarkable spectroscopic and magnetic properties, because they probably have practical applications as single-layer molecular devices; and we hope to materialize this type of LnMOFs using the mixed bridging ligands approach. In this paper the syntheses, crystal structures, luminescent and magnetic properties of three LnMOFs constructed from both nicotinate *N*-oxide (NNO^-) and glutarate (glu^{2-}), $\{[Ln(NNO)(glu)] \cdot 0.25H_2O\}_\infty$ (Ln = Eu, **1**; Ln = Gd, **2**; Ln = Dy, **3**), are presented. They are isostructural, exhibiting 2D layer network structures. It is notable that they are the first examples of 2D lanthanide(III) nicotinate *N*-oxide complexes containing acyclic binary carboxylic acids as the second bridging ligand. Interestingly, complex **1** shows fluorescent emissions while complex **3** displays field-induced

[a] *Beijing National Laboratory for Molecular Sciences, Center for Molecular Science, Key Laboratory of Organic Solids, Institute of Chemistry, Chinese Academy of Sciences, Beijing 100190, P. R. China; E-mail: cmliu@iccas.ac.cn*

Electronic Supplementary Information (ESI) available: X-ray crystallographic data for complexes **1**-**3** in CIF format, CCDC 1425344-1425342. Additional structural and magnetic characterization(Figures S1–S17 and Table S1 and S2). See DOI: 10.1039/x0xx00000x

two-step thermal magnetic relaxation. Such isostructural LnMOFs exhibiting luminescence and slow magnetic relaxation are quite rare in documents.

Experimental

Materials and methods

All chemicals are reagent grade, and obtained from commercial sources. The elemental analyses were determined on a Varlo ELIII elemental analyser. The infrared spectra were performed on a Bruker Tensor-27 spectrophotometer with pressed KBr pellets in the range 4000–400 cm^{-1}. The absorption spectrum was achieved on a Shimadzu UV-2600 spectrophotometer by using an integrating sphere. The X-ray powder diffraction (XRD) spectra were recorded on a Rigaku D/max 2500 diffractometer with Cu-Kα (λ = 1.5418 Å) radiation. The emission spectra in the solid state were measured on a HITACHI F-4500 luminescence spectrophotometer at room temperature. The solid state fluorescence lifetime was measured on Edinburgh Analytical Instruments F900. The absolute emission quantum yield was determined using a quantum yield measurement system C9920-02 from Hamamatsu at ambient temperature. The magnetic susceptibility measurements were carried out on a Quantum Design MPMS-XL5 SQUID magnetometer. Diamagnetic corrections were estimated from Pascal's constants of all components.

Synthetic procedures

A mixture of nicotinic acid *N*-oxide (1 mmol), glutaric acid (0.5 mmol), Ln_2O_3 (0.5 mmol) and H_2O (15 mL) in a 25 mL Teflon-lined stainless steel autoclave was maintained at 170 °C for 3 days. After the autoclave had cooled slowly to room temperature overnight, light yellow plate crystals of **1** (Ln = Eu, 75% yield based on Eu), or yellow plate crystals of **2** (Ln = Gd, 61% yield based on Gd), or light yellow plate crystals of **3** (Ln = Dy, 65% yield based on Dy) were harvested. These crystals were washed with water and dried at ambient temperature in air.

Elemental analysis (%): Calc. for $C_{11}H_{10.50}EuNO_{7.25}$ (**1**): C, 31.11; H, 2.49; N, 3.30. Found: C, 31.15; H, 2.53; N 3.26. IR (KBr pellet, cm^{-1}): 3445(b, s), 3130(w), 2980(w), 2925(w), 1623(m), 1580(s), 1454(w), 1405(m), 1288(w), 1222(w), 1124(w), 1062(w), 944(w), 813(m), 775(m), 675(m), 646(w), 572(w), 536(w), 508(w), 460(w).

Elemental analysis (%): Calc. for $C_{11}H_{10.50}GdNO_{7.25}$ (**2**): C, 30.36; H, 3.46; N, 3.26. Found: C, 30.32; H, 2.48; N 3.21. IR (KBr pellet, cm^{-1}): 3444(b, vs), 3131(w), 2979(w), 2929(w), 1624(m), 1580(s), 1454(w), 1407(m), 1289(w), 1222(w), 1125(w), 1063(w), 946(w), 815(m), 776(w), 675(w), 648(w), 573(w), 537(w), 512(w), 461(w).

Elemental analysis (%): Calc. for $C_{11}H_{10.50}DyNO_{7.25}$ (**3**): C, 30.36; H, 2.43; N, 3.22. Found: C, 30.40; H, 2.46; N, 3.18. IR (KBr pellet, cm^{-1}): 3449(b, s), 3131(w), 2980(w), 2941(w), 1622(m), 1582(s), 1456(w), 1407(s), 1313(w), 1288(w), 1222(w), 1126(w), 1063(w), 945(w), 815(m), 776(m), 675(m), 650(w), 573(w), 537(w), 516(w), 461(w).

Crystallography

A single crystal with dimensions 0.29 × 0.24 × 0.07 mm^3 of **1**, with dimensions 0.21 × 0.10 × 0.06 mm^3 of **2** and with dimensions 0.15 × 0.14 × 0.04 mm^3 of **3** was chose to collect data on a Rigaku ST Saturn 724+ diffractometer with *Mo-Kα* radiation (λ = 0.71073 Å) in the φ-scan mode. Cell parameters were reduced by the global refinement of the positions of all collected reflections. All three structures were solved by direct methods and refined with the ShelXL[14] refinement package using Least Squares minimisation. All non-hydrogen atoms were refined anisotropically, and all hydrogen atoms but those in the solvent hydrate molecule were set in calculated positions and refined as riding atoms. Selected crystallographic data and structure determination parameters for compounds **1**-**3** are summarized in Table 1.

Table 1. Crystal data and structural refinement parameters for complexes **1**-**3**.

	1	**2**	**3**
Chemical formula	$C_{11}H_{10.5}EuNO_{7.25}$	$C_{11}H_{10.5}GdNO_{7.25}$	$C_{11}H_{10.5}DyNO_{7.25}$
Formula weight	424.66	429.95	435.20
Crystal system	Monoclinic	Monoclinic	Monoclinic
Space group	*C2/c*	*C2/c*	*C2/c*
a/Å	11.546(2)	11.577(2)	11.523(2)
b/Å	11.409(2)	11.357(2)	11.262(2)
c/Å	18.075(4)	18.158(4)	18.197(4)
β/°	92.06(3)	91.35(3)	90.67(3)
V/$Å^3$	2379.7(8)	2386.7(8)	2361.4(8)
Z	8	8	8
T/K	173(2)	293(2)	293(2)
λ(Mo-Kα)/Å	0.71073	0.71073	0.71073
ρ_{calc}/g · cm^{-3}	2.371	2.393	2.448
μ(Mo-Kα)/mm^{-1}	5.308	5.594	6.365
ϑ range	3.33°≤θ≤27.46°	3.34°≤θ≤27.51°	3.36°≤θ≤27.49°
F(000)	1636	1644	1660
Limiting indices	−14≤*h*≤14, −11≤*k*≤14, −23≤*l*≤16	−15≤*h*≤15, −14≤*k*≤14, −23≤*l*≤23	−14≤*h*≤13, −13≤*k*≤14, −21≤*l*≤23
Reflections collected	7690	9057	7884
Independent reflections	2705	2732	2691
$R_1{}^a$ [$I > 2\sigma(I)$]	0.0241	0.0270	0.0347
$_wR_2{}^b$ [$I > 2\sigma(I)$]	0.0549	0.0535	0.0701
$R_1{}^a$ [all data]	0.0248	0.0291	0.0372
$_wR_2{}^b$ [all data]	0.0552	0.0543	0.0712
S	1.138	1.154	1.163

$^aR_1 = \sum||Fo|-|Fc|| / \sum|Fo|$, $^b{}_wR_2 = \sum\{[w(Fo^2-Fc^2)^2] / \sum[wFo^2]^2\}^{1/2}$

Results and discussion

Preparation and XRD spectra

Nicotinate *N*-oxide had been used to construct some lanthanide(III) complexes by several groups, most of them are LnMOFs.[15] The second bridging ligand was often applied to assembly high-dimensional lanthanide(III) complexes, despite of the unavoidable coordination competition betwee

the two types of bridging ligands. The most common second bridging ligand is oxalate, which has been successfully used to prepare a lot of lanthanide(III) LnMOFs with mixed bridges,[12b,12d,16] including a 3D europium(III) nicotinate *N*-oxide complex.[15c] However, the case of adopting other acyclic binary carboxylates as the second bridging ligand for the construction of LnMOFs is quite limited.[15c] We think the reason is that the adaptation of the two types of carboxylate ligands is very difficult, and there exists the coordination contest between the two types of bridging ligands. In this study, we adopted glutarate as the second bridging ligand to assembly the lanthanide(III) nicotinate *N*-oxide complexes, and three 2D layer LnMOFs **1**-**3** were obtained. When other acyclic binary carboxylates such as malonate, succinate, hexanedioate and heptanedioate were used as the reactant instead of glutarate, crystalline products would be fruitless, which suggests that only glutarate can match with nicotinate *N*-oxide to prepare the 2D layer LnMOFs.

The purity of compounds **1**-**3** were examined by their powder XRD spectra. The XRD spectrum pattern and the corresponding pattern simulated on the basis of the single-crystal structure can match well in positions of diffraction peaks (Fig. S1-S3,† supporting Information). This indicates that the samples as synthesized are pure enough for the spectroscopic and magnetic properties' study.

Crystal structures

The X-ray single crystal analyses revealed that complexes **1**, **2** and **3** are isostructural, and they crystallize in the space group *C*2/*c*. Therefore, the dysprosium(III) species is described here in details as the representation. As shown in Fig. 1, the dysprosium(III) ions of **3** are connected with each other through not only the double bridges of antiparallel nicotinate *N*-oxide anions but also the double bridges of antiparallel glutarate anions, generating an extended 2D layer network parallel to the *ab* plane.

The Dy1 atom is nine-coordinated, bonded by two oxygen atoms from the same carboxylate group of the glutarate anion, two oxygen atoms from the same carboxylate group of the nicotinate *N*-oxide anion, three carboxylate oxygen atoms from three glutarate anions, and two *N*-oxide oxygen atoms from two nicotinate *N*-oxide anions. The Dy1-O bond distances [2.321(4)-2.624(4) Å] are in the normal range (Table 2).[9,12c,12d,13] Shape software[17] was used to analyse the exact geometry of the Dy1 atom, the results revealed that the configuration of the nine-coordinated Dy1 ion is close to the spherical capped square antiprism (with the deviation of 1.913 from the ideal C_{4v} symmetry), but it should be best described as the muffin (with the deviation of 1.711 from the ideal C_s symmetry) (Table S1, Supporting Information).

Table 2. Selected bond distances(Å) and angles(°) for **1**-**3**.

		1	
Eu1-O1[1]	2.466(3)	Eu1-O1[2]	2.526(3)
Eu1-O2	2.429(3)	Eu1-O3	2.600(3)
Eu1-O4	2.372(3)	Eu1-O5[3]	2.368(3)
Eu1-O6[1]	2.452(3)	Eu1-O7[4]	2.368(3)
Eu1-O7[1]	2.617(3)	O2-Eu1-1O3	52.00(8)
O6[1]-Eu1-O7[1]	50.97(8)	O1[1]-Eu1-O1[2]	63.03(10)
		2	
Gd1-O1[1]	2.456(3)	Gd1-O1[2]	2.524(3)
Gd1-O2	2.412(3)	Gd1-O3	2.619(3)
Gd1-O4	2.357(3)	Gd1-O5[3]	2.357(3)
Gd1-O6[1]	2.440(3)	Gd1-O7[4]	2.355(3)
Gd1-O7[1]	2.621(3)	O2-Gd1-1O3	51.71(10)
O6[1]-Gd1-O7[1]	50.91(9)	O1[1]-Gd1-O1[2]	62.71(11)
		3	
Dy1-O1[1]	2.428(3)	Dy1-O1[2]	2.501(4)
Dy1-O2	2.380(4)	Dy1-O3	2.619(5)
Dy1-O4	2.325(4)	Dy1-O5[3]	2.322(4)
Dy1-O6[1]	2.394(4)	Dy1-O7[4]	2.321(4)
Dy1-O7[1]	2.624(4)	O2-Dy-1O3	51.84(13)
O6[1]-Dy1-O7[1]	51.09(12)	O1[1]-Dy1-O1[2]	62.42(14)

Symetry Codes: ([1] 1/2+X, 1/2+Y, Z; [2] 1/2−X, −1/2−Y, 1−Z; [3] 1/2−X, 1/2−Y, 1−Z; [4] −X, −Y,1−Z).

Each nicotinate *N*-oxide ligand links two Dy atoms with its μ^2-bridging *N*-oxide moiety and the third Dy atom with its two carboxylic oxygen atoms, adopting a tri-connecter coordination mode (Scheme 1a), the Dy…Dy separation bridged by the *N*-oxide moiety is 4.216 Å. Nevertheless, the glutarate anion coordinates to four Dy atoms with a tetra-connecter mode (Scheme 1b), in which one carboxylic group synchronously serves as a bidentate chelating ligand to one Dy^{3+} ion and as a monodentate ligand to the neighbouring Dy^{3+} ion, with the corresponding Dy…Dy separation of 4.007 Å, while another carboxylate group links other two lanthanide ions as a bismonodentate bridge.

In the layer network of **3**, parallel $[DyO_2(CO_2)_4]$ chains are formed through bridging the Dy atoms by alternative double *N*-oxide groups from two nicotinate *N*-oxide anions and quadruple carboxylate groups from four glutarate anions. These chains are set off not only by the pyridine ring of the nicotinate *N*-oxide ligand but also by the propane group of the glutarate ligand. This is why only the glutarate ligand can match with the nicotinate *N*-oxide ligand to construct the 2D layer LnMOF complexes **1**-**3**.

Compounds **1** and **2** are of the same structure as **3** (Fig. S4 and Fig. S5). As shown in Table 2, the average Ln–O bond lengths decrease from **1** [2.470(3) Å for Eu1] to **2** [2.460(3) Å for Gd1] to **3** [2.430(2) Å for Dy1], in good agreement with the radius contraction from the europium(III) ion to the dysprosium(III) ion.

Luminescent properties

The photoluminescence properties of complex **1** were investigated in solid state at room temperature. As shown in Fig. 2, the excitation spectrum (λ_{em} = 615 nm) of complex **1** displays the characteristic absorption bands of the Eu^{3+} ion at 396 and 467 nm. Its emission spectra excited by 400 nm UV light exhibit some characteristic transition of the Eu^{3+} ion. The peaks at 590, 614 and 695 nm are assigned to the $^5D_0 \rightarrow {}^7F_1$, $^5D_0 \rightarrow {}^7F_2$ and $^5D_0 \rightarrow {}^7F_4$ transitions, respectively. The most intense emitting band is the $^5D_0 \rightarrow {}^7F_2$ transition at 614 nm, which dominates the red emission light. Furthermore, the intensity of

the $^5D_0 \rightarrow {}^7F_2$ transition, which belongs to an electric dipole transition, is stronger than that of the $^5D_0 \rightarrow {}^7F_1$ transition, an magnetic dipole transition. This indicates asymmetry of the coordination environment of the Eu^{3+} ion,[18] as aforementioned in the crystallographic structure section. In addition, the $^5D_0 \rightarrow {}^7F_0$ and $^5D_0 \rightarrow {}^7F_3$ transitions at around 580 and 650 nm, respectively, are very weak; the absolute emission quantum yield of **1** is only 0.055, and its fluorescence lifetime is 4.2 ns (Fig. S6), all these results suggest that the luminescence intensity of **1** is not very strong, which could be ascribed to the oscillation of coordination water molecules and solvent water molecules, partially quenching the luminescence.[19]

The absorption spectrum in solid state of **1** shows a broad band at around 380 nm (Fig. S7), which matches the 396 nm peak in the excitation spectrum (λ_{em} = 615 nm) (Fig. 2), indicating that the indirect population of the $^5D_0$ luminescent excited states is attributed to an overall energy transfer from the organic ligand to the europium(III) ion,[20] and the nicotinate *N*-oxide ligand in **1** indeed acts as a conduit for the photoluminescence process.

Magnetic properties

Direct current (dc) magnetic susceptibilities of complexes **2** and **3** were measured using microcrystalline powdered samples under an applied field of 1 kOe in the temperature range of 2–300 K. As shown in Fig. 3, the χT product of **2** at 300 K (7.93 cm^3Kmol^{-1}) is slightly larger than the spin-only value (7.88 cm^3Kmol^{-1}) of one Gd^{3+} ion (S = 7/2, L = 0, g = 2). Above 10 K, the decline of the χT value with decreased temperature is slow, it then becomes fast upon further chilling. The $1/\chi$ versus T plot of **2** in the temperature range of 300–100 K obeys the Curie–Weiss law, $1/\chi = (T-\vartheta)/C$, affording the Curie constant C of 8.09 cm^3Kmol^{-1} and the Weiss constant ϑ of −9.81 K (Fig. S8). The small negative ϑ value suggests the weak antiferromagnetic interaction among the Gd^{3+} ions in **2**. The χT value of **3** at room temperature (14.13 cm^3Kmol^{-1}) is consistent with that expected (14.17 cm^3Kmol^{-1}) for one spin-only Dy^{3+} ion (S = 5/2, L = 5, $^6H_{15/2}$, g = 4/3). It is almost invariable in the temperature range of 300–100 K, but falls precipitously below 50 K, and finally reaches a value of 7.13 cm^3Kmol^{-1} at 2K. The diminishment of the χT value upon cooling of **3** is thus due to not only the weak antiferromagnetic interaction similar to **2**, but also the depopulation of the Dy^{3+} Stark sublevels caused by the ligand field.[9]

The field dependence of the magnetization of **2** and **3** were determined at 2-6 K. The reduced M versus H/T plots of **3** are obviously non-superimposed (Fig. S9), which suggests that complex **3** has a strong magnetic anisotropy, being propitious to show the SMM behaviours. Comparatively, the isofield lines of **2** are almost superimposable due to a weak magnetic anisotropy (Fig. S10).

Alternating-current (ac) magnetic susceptibility was then determined to investigate the SMM behaviours of **3**. When the dc field was zero, the out-of-phase (χ'') signals appeared in the ac susceptibility of **3** (Fig. S11), but no peak could be observed, which suggests the existence of quantum effects, strongly influencing the magnetic relaxation process. Therefore, a dc field of 2000 Oe was applied, now both the χ' and χ'' signals in the ac susceptibility of **3** are strongly frequency dependent below 7 K, and peaks appeared in all χ'' versus T curves at different frequencies (1-1500 Hz) (Fig. 4), which indicates that the dc field of 2000 Oe can eliminate the ground-state degeneracy and cut the quantum-tunnelling effects effectively.

In order to evaluate the effective thermal barrier(U_{eff}) of the magnetic relaxation, the peak temperatures at different ac oscillating frequencies were presented as the formation of $\ln(\tau)$-$1/T$ plots, which then were fitted by the Arrhenius law, $\tau = \tau_0 \exp(U_{eff}/k_BT)$ (τ is the magnetization relaxation time) (Fig. S12). The U_{eff}/k_B value of **3** was calculated to be 44.2(1.8) K; and the τ_0 value equals to $2.3(0.2)\times10^{-8}$ s, which is in the normal range of 10×10^{-6}-10×10^{-11} s for the SMMs or the SIMs.[9,10] Furthermore, the ϕ value of **3** was figured up to be 0.26 by equation $\phi = (\Delta T_f/T_f)/\Delta(\log f)$ (f is the frequency),[21] which is in agreement with the value for a superparamagnet (ϕ > 0.1) but quite larger than that for a spin glass ($\phi \approx$ 0.01),[21] confirming the SMM behaviours of **3**.

The frequency-dependent ac susceptibilities were also measured under a dc field of 2000 Oe to deeply study the magnetization dynamics of **3**. The corresponding χ'' versus χ' plots at 2-5 K are depicted as Fig. 5, such Cole–Cole plots exhibit half-baked semicircular characteristic, indicating that there exist two magnetic relaxation processes in **3**: the fast relaxation phase (FR) and the slow relaxation phase (SR), which correspond to the left part and the right part of the Cole–Cole curves. These Cole–Cole plots could be well fitted by the sum of two modified Debye functions (equ 1):[13d, 13e, 22]

$$\chi_{ac}(\omega) = \frac{\chi_2 - \chi_1}{1 + (i\omega\tau_2)^{(1-\alpha_2)}} + \frac{\chi_1 - \chi_0}{1 + (i\omega\tau_1)^{(1-\alpha_1)}} + \chi_0 \qquad (1)$$

Fig. 5 and Figs. S13-S16 show the calculation results visually. As listed in Table S2, the α_2 values of 0.0002-0.11 are smaller than the α_1 values of 0.71–0.55 at 2-5 K, which suggests that distribution of the relaxation time for the SR phase is narrower with respect to the FR phase. As described above, only one crystallographically independent dysprosium(III) ion exists in **3**, so the two-step thermal magnetic relaxation should be attributed to the field-inducing role,[23] such a case is the first time observed in the high-dimensional DyMOF systems. Additionally, there is no any hysteresis in the M versus H plot of **3** at 1.9 K (Fig. S17).

Because the antiferromagnetic interaction among the Dy^{3+} ions in **3** is very weak, as suggested by that among the Gd^{3+} ions in **2**, the electrostatic model implemented in the Magellan program[24] was adopted to illuminate the magnetic anisotropy of **3**. As shown in Fig. 6, the calculated magnetic easy axis is very close to the direction defined by the Dy^{3+} ion and the pyridine ring center of the nicotinate *N*-oxide anion through its carboxylate group, with a small separation angle of 5.47°. In the total layer network of **3**, all the magnetic axes of the dysprosium(III) ions are arranged in an antiparallel mode. Such an arrangement of the magnetic easy axes favours the SMM behaviours of **3**.

The magnetocaloric effect (MCE) of **2** was examined by magnetic entropy changes ($-\Delta S_m$), which were calculated by using the Maxwell relation $\Delta S_m(T)_{\Delta H} = \int[\partial M(T,H)/\partial T]_H dH$.[25] As shown in Fig. 7 in the $-\Delta S_m$ versus T curve format, the $-\Delta S_m$ value increases as the

ΔH value is increased. The largest $-\Delta S_m$ value for the maximum ΔH of 50 kOe at 2 K is only 1.84 $Jkg^{-1}K^{-1}$, which is not large enough for **2** to be a nice candidate for the cryogenic magnetic refrigeration materials.

Conclusions

In summary, the "mixed bridging ligands" strategy has been successfully applied to synthesize three isostructural 2D LnMOFs, which are constructed from both the nicotinate *N*-oxide anion and the glutarate anion. The gadolinium(III) complex is antiferromagnetic. The dysprosium(III) species displays the SMM behaviours, showing two-step thermal magnetic relaxation under a 2k Oe dc field; while the europium(III) analogue exhibits fluorescent properties, with typical narrow emission bands of the lanthanide ion. To the best of our knowledge, only few examples of isostructural LnMOFs can exhibit luminescence and slow magnetic relaxation,[11i] our work represents the first one with mixed bridging ligands. This work demonstrates that the "mixed bridging ligands" strategy is a promising approach to isostructural LnMOFs, which can show interesting spectroscopic or magnetic properties, depending on the lanthanide ions used.

Acknowledgements

This work was supported by National Key Basic Research Program of China (2013CB933403), National Natural Science Foundation of China (21471154, 21073198 and 91022014), and the Strategic Priority Research Program of the Chinese Academy of Sciences (XDB12010103). We thank Prof. Chun-Xi Zhang for help with the fluorescence measurements.

Notes and references

1 (a) J. Rocha, L. D. Carlos, F. A. A. Paza and D. Ananias, *Chem. Soc. Rev.*, 2011, **40**, 926; (b) Y. Hasegawa and T. Nakanishi, *RSC Adv.*, 2015, **5**, 338.

2 (a) Z. Amghouz, L. Roces, S. García-Granda, J. R. Garcia, B. Souhail, L. Mafra, F. N. Shi and J. Rocha, *Inorg. Chem.*, 2010, **49**, 7917; (b) S. M. F. Vilela, D. Ananias, J. A. Fernandes, P. Silva, A. C. Gomes, N. J. O. Silva, M. O. Rodrigues, J. P. C. Tomé, A. A. Valente, P. Ribeiro-Claro, L. D. Carlos, J. Rocha and F. A. A. Paz, *J. Mater. Chem. C.*, 2014, **2**, 3311.

3 H. Li, W. Shi, K. Zhao, Z. Niu, H. Li and P. Cheng, *Chem.–Eur. J.*, 2013, **19**, 3358.

4 (a) D.-X. Xue, Y. Belmabkhout, O. Shekhah, H. Jiang, K. Adil, A. J. Cairns and M. Eddaoudi, *J. Am. Chem. Soc.*, 2015, **137**, 5034; (b) A. H. Assen, Y. Belmabkhout, K. Adil, P. M. Bhatt, D.-X. Xue, H. Jiang and M. Eddaoudi, *Angew. Chem. Int. Ed.*, 2015, **54**, 1.

5 Y. Cui, B. Chen and G. Qian, *Coord. Chem. Rev.*, 2014, **273**, 76.

6 G. Li, T. Akitsu, O. Sato and Y. Einaga, *J. Am. Chem. Soc.*, 2003, **125**, 12396.

7 (a) B. L. Chen, Y. Yang, F. Zapata, G. N. Lin, G. D. Qian and E. B. Lobkovsky, *Adv. Mater.*, 2007, **19**, 1693; (b) B. V. Harbuzaru, A. Corma, F. Rey, J. L. Jordá, D. Ananias, L. D. Carlos and J. Rocha, *Angew. Chem. Int. Ed.*, 2009, **48**, 6476; (c) K.-L. Wong, G.-L. Law, Y.-Y. Yang and W.-T. Wong, *Adv. Mater.*, 2006, **18**, 1051; (d) G. Lu and J. T. Hupp, *J. Am. Chem. Soc.*, 2010, **132**, 7832.

8 (a) N. Sabbatini, M. Guardigli and J. M. Lehn, *Coord. Chem. Rev.*, 1993, **123**, 20; (b) E. G. Moore, A. P. S. Samuel and K. N. Raymond, *Acc. Chem. Res.*, 2009, **42**, 542; (c) K. Binnemans, *Chem. Rev.*, 2009, **109**, 4283; (d) Y.-J. Cui, Y.-F. Yue, G.-D. Qiang and B.-L. Chen, *Chem. Rev.*, 2012, **112**, 1126.

9 (a) D. N. Woodruff, R. E. P. Winpenny and R. A. Layfield, *Chem. Rev.*, 2013, **113**, 5110; (b) P. Zhang, Y.-N. Guo and J.k. Tang, *Coord. Chem. Rev.*, 2013, **257**, 1728.

10 (a) R. Sessoli, D. Gatteschi, A. Caneschi and M. A. Novak, *Nature*, 1993, **365**, 141; (b) D. Gatteschi and R. Sessoli, *Angew. Chem. Int. Ed.*, 2003, **42**, 268; (c) G. Christou, D. Gatteschi, D. N. Hendrickson and R. Sessoli, *MRS Bull.*, 2000, **25**, 66; (d) C. Benelli and D. Gatteschi, *Chem. Rev.*, 2002, **102**, 2369; (e) L. M. C. Beltran and J. R. Long, *Acc. Chem. Res.*, 2005, **38**, 325; (f) G. Aromi and E. K. Brechin, *Struct. Bonding*, 2006, **122**, 1; (g) R. Bagai and G. Christou, *Chem. Soc. Rev.*, 2009, **38**, 1011; (h) V. Chandrasekhar and Murugesapandian, *Acc. Chem. Res.*, 2009, **42**, 1047; (i) R. Sessoli and A. K. Powell, *Coord. Chem. Rev.*, 2009, **253**, 232[illegible]; (j) M. Murrie, *Chem. Soc. Rev.* 2010, **39**, 1986; (k) G. E. Kostakis, A. M. Akoab and A. K. Powell, *Chem. Soc. Rev.*, 201[illegible] **39**, 2238; (l) R. Vincent, S. Klyatskaya, M. Ruben, W. Wernsdorfer and F. Balestro, *Nature*, 2012, **488**, 357; (m) T. Komeda, H. Isshiki, J. Liu, Y.-F. Zhang, N. Lorente, K. Katoh, B. K. Breedlove and M. Yamashita, *Nat. Comm.*, 2011, **2**, 217; (n) B.-W. Wang, X.-Y. Wang, H.-L. Sun, S.-D. Jiang and S. Gao, *Philos. Trans. R. Soc. A*, 2013, **371**, 20120316; (o) K. Liu, W. Shi and P. Cheng, *Coord. Chem. Rev.*, 2015, **289-290**, 74.

11 (a) D. Savard, P. H. Lin, T. J. Burchell, I. Korobkov, W. Wernsdorfer, R. Clérac and M. Murugesu, *Inorg. Chem.*, 2009, **48**, 11748; (b) X. Yi, K. Bernot, G. Calvez, C. Daiguebonne and O. Guillou, *Eur. J. Inorg. Chem.*, 2013, 5879; (c) F. R. Fortea-Perez, J. Vallejo, M. Julve, F. Lloret, G. De Munno, D. Armentano and E. Pardo, *Inorg. Chem.*, 2013, **52**, 4777; (d) M. Chen, E. C. Sañudo, E. Jiménez, S.-M. Fang, C.-S. Liu and M. Du, *Inorg. Chem.*, 2014, **53**, 6708; (e) P. F. Shi, Y. Z. Zheng, X. Q. Zhao, G. Xiong, B. Zhao, F. F. Wan and P. Cheng, *Chem. Eur. J.*, 2012, **18**, 15086; (f) Q.-Y. Liu, Y.-L. Li, Y.-L. Wang, C.-M. Liu, L.-W. Ding and Y. Liu, *CrystEngComm*, 2014, **16**, 486; (g) D.-D. Yin, Q. Chen, Y.-S. Meng, H.-L. Sun, Y.-Q. Zhang and S. Gao, *Chem. Sci.*, 2015, **6**, 3095; (h) X. Yi, G. Calvez, C. Daiguebonne, O. Guillou and Kevin Bernot, *Inorg. Chem.*, 2015, **54**, 5213; (i) J. Zhao, G.-H. Zhu, L.-Q. Xie, Y.-S. Wu, H.-L. Wu, A.-J. Zhou, Z.-Y. Wu, J. Wang, Y.-C. Chen and M.-L. Tong, *Dalton Trans.*, 2015, **44**, 14424; (j) X. Ma, N. Xu, C. Gao, L. Li, B. Wang, W. Shi and P. Cheng, *Dalton Trans.*, 2015, **44**, 5276; (k) Q. Li and S. Du, *RSC Adv.*, 2015, **5**, 9898.

12 (a) C.-M. Liu, J.-L. Zuo, D.-Q. Zhang and D.-B. Zhu, *CrystEngComm*, 2008, **10**, 1674; (b) C.-M. Liu, M. Xiong, D.-Q. Zhang, M. Du and D.-B. Zhu, *Dalton Trans.*, 2009, 5666; (c) C.-M. Liu, D.-Q. Zhang and D.-B. Zhu, *RSC Adv.*, 2014, **4**, 36053; (d) C.-M. Liu, D.-Q. Zhang and D.-B. Zhu, *RSC Adv.*, 2015, **5**, 63186.

13 (a) C.-M. Liu, D.-Q. Zhang, X. Hao and D.-B. Zhu, *Cryst. Growth Des.*, 2012, **12**, 2948; (b) X.-L. Li, C.-L. Chen, Y.-L. Gao, C.-M. Liu, X.-L. Feng, Y.-H. Gui and S.-M. Fang, *Chem.– Eur. J.*, 2012, **18**, 14632; (c) C.-M. Liu, D.-Q. Zhang and D. B. Zhu, *Dalton Trans.*, 2010, **39**, 11325; (d) C.-M. Liu, D.-Q. Zhang and D. B. Zhu, *Inorg. Chem.*, 2013, **52**, 8933; (e) C.-M. Liu, D.-Q. Zhang and D. B. Zhu, *Dalton Trans.*, 2013, **42**, 14813; (f) C.-M. Liu, D.-Q. Zhang, X. Hao and D.-B. Zhu, *Chem.–Asian J.*, 2014, **9**, 1847.

14 G.M. Sheldrick, *Acta Cryst.*, 2008, **A64**, 112.

15 (a) Z. He, Z.-M. Wang and C.-H. Yan, *CrystEngComm.*, 2005, **7**, 143; (b) J.-G. Mao, H.-J. Zhang, J.-Z. Ni, S.-B. Wang and T.C.W.

Mak, *Polyhedron*, 1998, **17**, 3999; (c) L. Zhang, D. Xu, Y. Zhou and F. Jiang, *New J. Chem*., 2010, **34**, 2470.

16 (a) R. Vaidhyanathan, S. Natarajan and C. N. R. Rao, *Inorg. Chem.*, 2002, **41**, 4496; (b) B. Li, W. Gu, L.-Z. Zhang, J. Qu, Z.-P. Ma, X. Liu and D.-Z. Liao, *Inorg. Chem.*, 2006, **45**, 10425; (c) L. Cañadillas-Delgado, J. Pasán, O. Fabelo, M. Hernández-Molina, F. Lloret, M. Julve and C. Ruiz-Pérez, *Inorg. Chem.*, 2006, **45**, 10585; (d) W.-H. Zhu, Z.-M. Wang and S. Gao, *Inorg. Chem.*, 2007, **46**, 1337; (e) T.-F. Liu, W.j. Zhang, W.-H. Sun and R. Cao, *Inorg. Chem.*, 2011, **50**, 5242; (f) A.-H. Yang, J.-Y. Zou, W.-M. Wang, X.-Y. Shi, H.-L. Gao, J.-Z. Cui and B. Zhao, *Inorg. Chem.*, 2014, **53**, 7092; (g) M.-S. Liu, Q.-Y. Yu, Y.-P. Cai, C.-Y. Su, X.-M. Lin, X.-X. Zhou and J.-W. Cai, *Cryst. Growth Des.*, 2008, **8**, 4083; (h) H. Wang , S.-J. Liu, D. Tian, J.-M. Jia and T.-L. Hu, *Cryst. Growth Des.*, 2012, **12**, 3263; (i) Z.-P. Deng, W. Kang, L.-H. Huo, H. Zhao and S. Gao, *Dalton Trans*., 2010, **39**, 6276; (j) X. Feng, X.-L. Ling, L. Liu, H.-L. Song, L.-Y. Wang, S.-W. Ng and B.-Y. Su, *Dalton Trans.*, 2013, **42**, 10292; (k) Q.-F. Yang, Y. Yu, T.-Y. Song, J.-H. Yu, X. Zhang, J.-Q. Xu and T.-G. Wang, *CrystEngComm*, 2009, **11**, 1642; (l) Y.-H. Zhang, X. Li, S. Song, H.-Y. Yang, D. Ma and Y.-H. Liu, *CrystEngComm*, 2014, **16**, 8390.

17 D. Casanova, M. Llunell, P. Alemany and S. Alvarez, *Chem.–Eur. J.*, 2005, **11**, 1479.

18 (a) Y. G. Sun, X. F. Gu, F. Ding, P. F. Smet, E. J. Gao, D. Poelman and F. Verpoort, *Cryst. Growth Des*., 2008, **8**, 1059; (b) S. Petit, F. Baril-Robert, G. Pilet, C. Reber and D. Luneau, *Dalton Trans*., 2009, 6809; (c) Z.-P. Deng, W. Kang, L.-H. Huo, H. Zhao and S. Gao, *Dalton Trans*., 2010, **39**, 6276.

19 B. Zhao, X. Y. Chen, P. Cheng, D. Z. Liao, S. P. Yan and Z. H. Jiang, *J. Am. Chem. Soc.*, 2004, **126**, 15394.

20 D. J. Lewis, F. Moretta, A. T. Holloway and Z. Pikramenou, *Dalton Trans*., 2012, **41**, 13138.

21 J. A. Mydosh, *Spin Glasses, An Experimental Introduction*, Taylor and Francis, London, 1993.

22 (a) M. Grahl, J. Kotzler and I. Sessler, *J. Magn. Magn. Mater*., 1990, **90–91**, 187; (b) Y.-N. Guo, G.-F. Xu, P. Gamez, L. Zhao, S.-Y. Lin, R. Deng, J. Tang and H.-J. Zhang, *J. Am. Chem. Soc.*, 2010, **132**, 8538.

23 (a) M. Jeletic, P. H. Lin, J. J. L. Roy, I. Korobkov, S. I. Gorelsky and M. Murugesu, *J. Am. Chem. Soc*., 2011, **133**, 19286; (b) J. Ruiz, A. J. Mota, A. Rodríguez-Diéguez, S. Titos, J. M. Herrera, E. Ruiz, E. Cremades, J. P. Costes and E. Colacio, *Chem. Commun*., 2012, **48**, 7916; (c) F. Habib, J. Long, P.-H. Lin, I. Korobkov, L. Ungur, W. Wernsdorfer, L. F. Chibotaruc and M. Murugesu, *Chem. Sci.*, 2012, **3**, 2158; (d) X.-L. Li, C.-L. Chen, H.-P. Xiao, A.-L. Wang, C.-M. Liu, X.j. Zheng, L.-J. Gao, X.-G. Yang and S.-M. Fang, *Dalton Trans.*, 2013, **42**, 15317.

24 N. F. Chilton, D. Collison, E. J. L. McInnes, R. E. P. Winpenny and A. Soncini, *Nat. Commun*., 2013, **4**, 2551.

25 V. K. Pecharsky and K. A. Gschneidner, Jr., *J. Magn. Magn. Mater.*, 1999, **200**, 44.

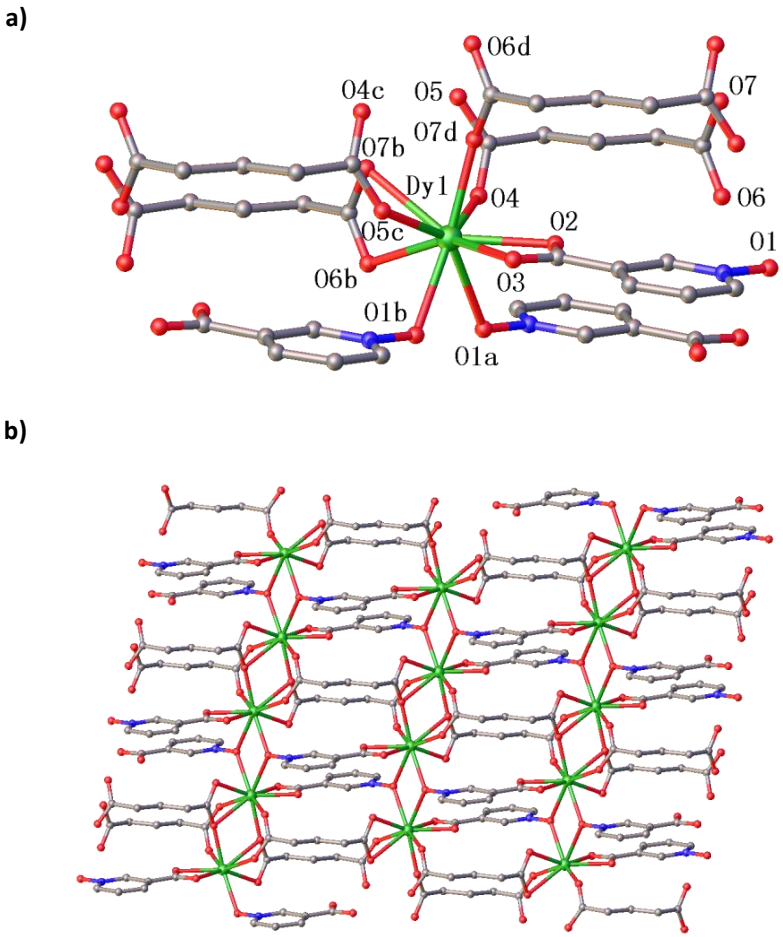

Fig. 1. The coordination environment of the Dy atom in **3** (a), symmetry codes: a: 1/2−x, −1/2−y, 1−z; b: 1/2+x, 1/2+y, z; c: 1/2−x, 1/2−y, 1−z; d: −x, −y, 1−z; and 2D layer structure of **3** viewed down the *c*-axis (b).

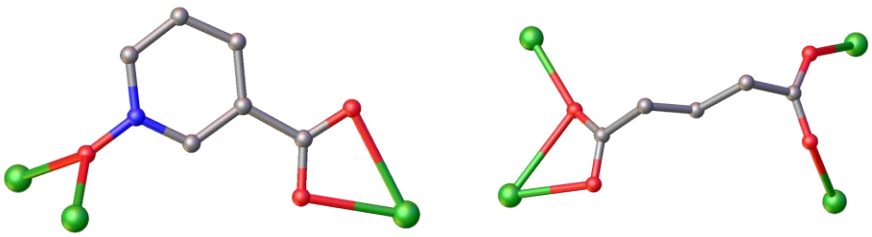

Scheme 1. The coordination modes of nicotinate *N*-oxide (a) and glutarate (b) in **3**.

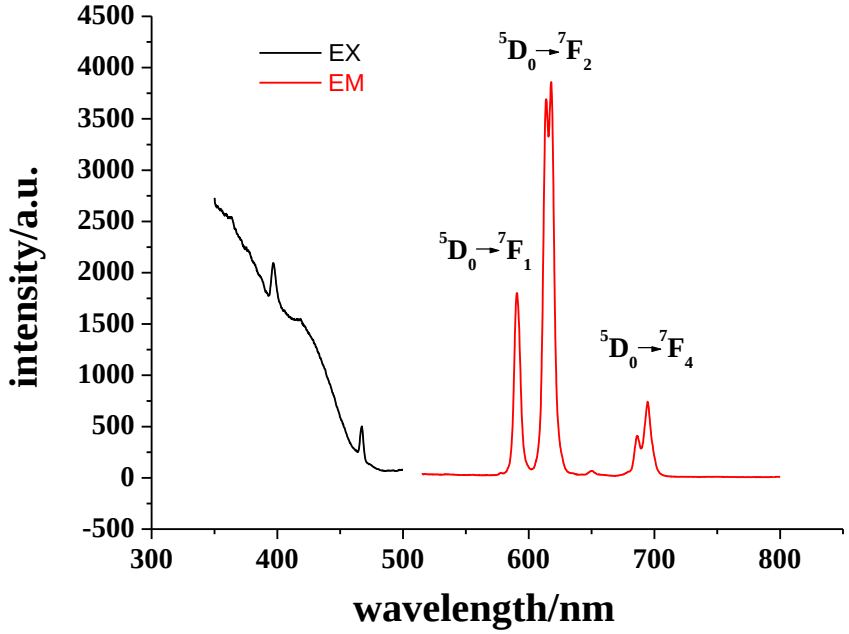

Fig. 2. Excitation spectrum (λ_{em}= 615 nm) and emission spectrum (λ_{ex} = 400 nm) in the solid state at room temperature for complex **1**.

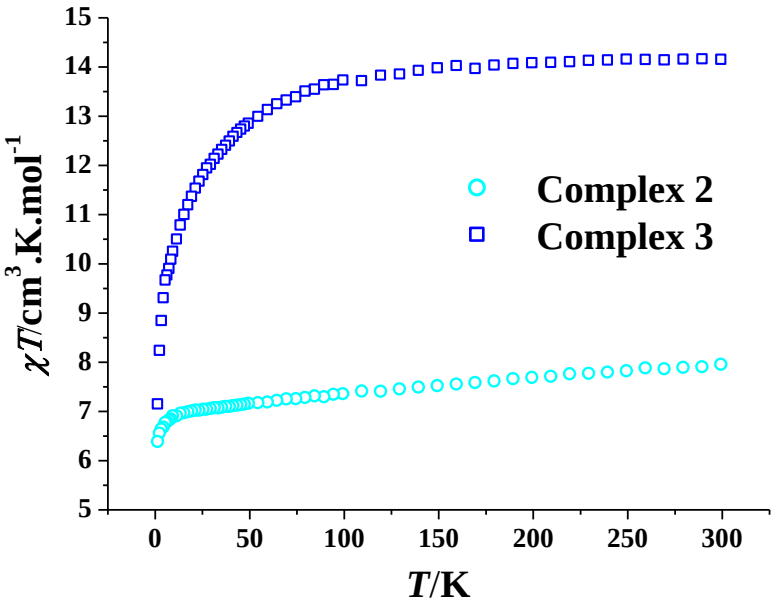

Fig. 3. Plots of χT versus T of complexes **2** and **3**.

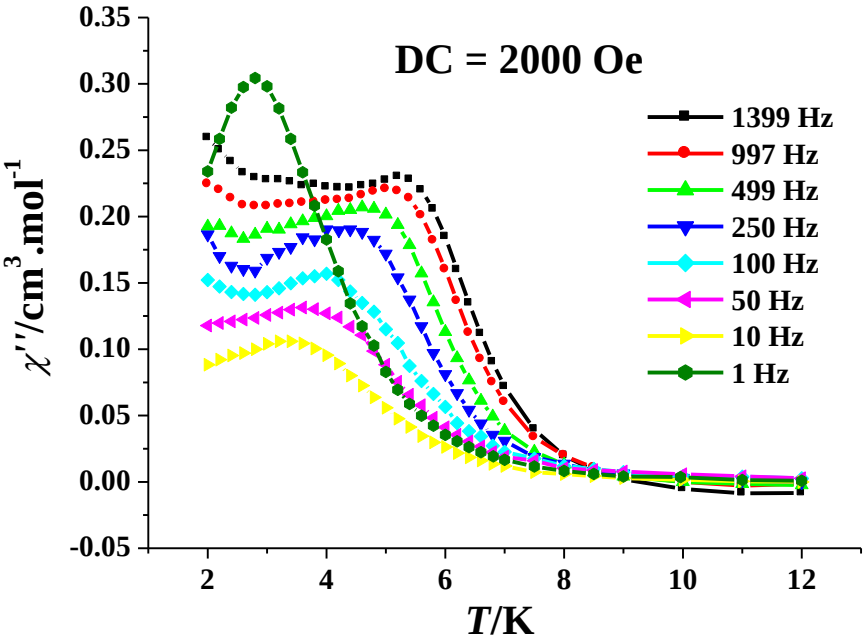

Fig. 4. The out-of-phase (χ'') ac susceptibility signals measured in a 2.5 Oe oscillating field with a 2 kOe dc field for **3**.

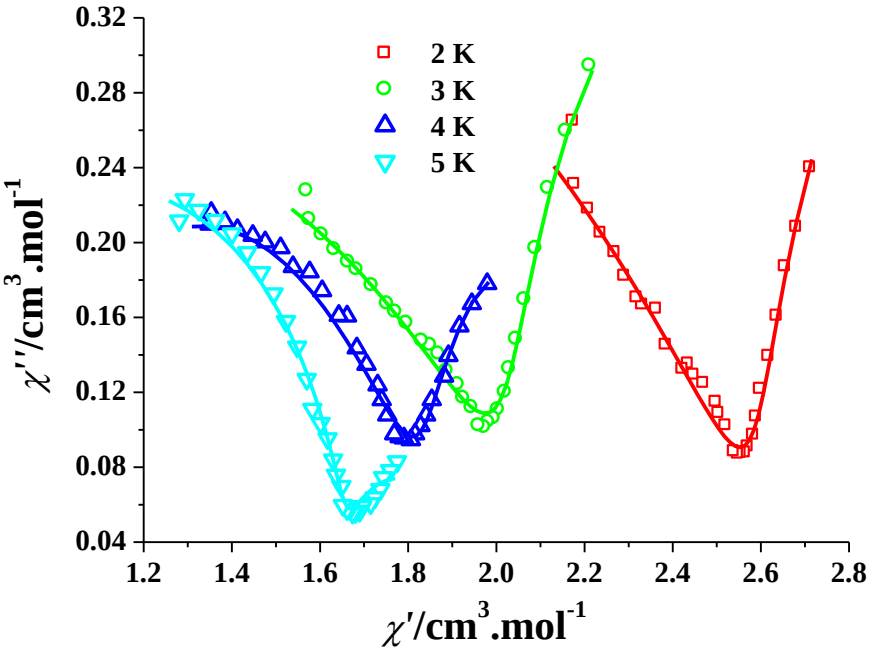

Fig. 5. Cole–Cole plots at 2–5 K for **3** (H_{dc} = 2 kOe and H_{ac} = 2.5 Oe). The solid lines represent the best fitting with the sum of two modified Debye function

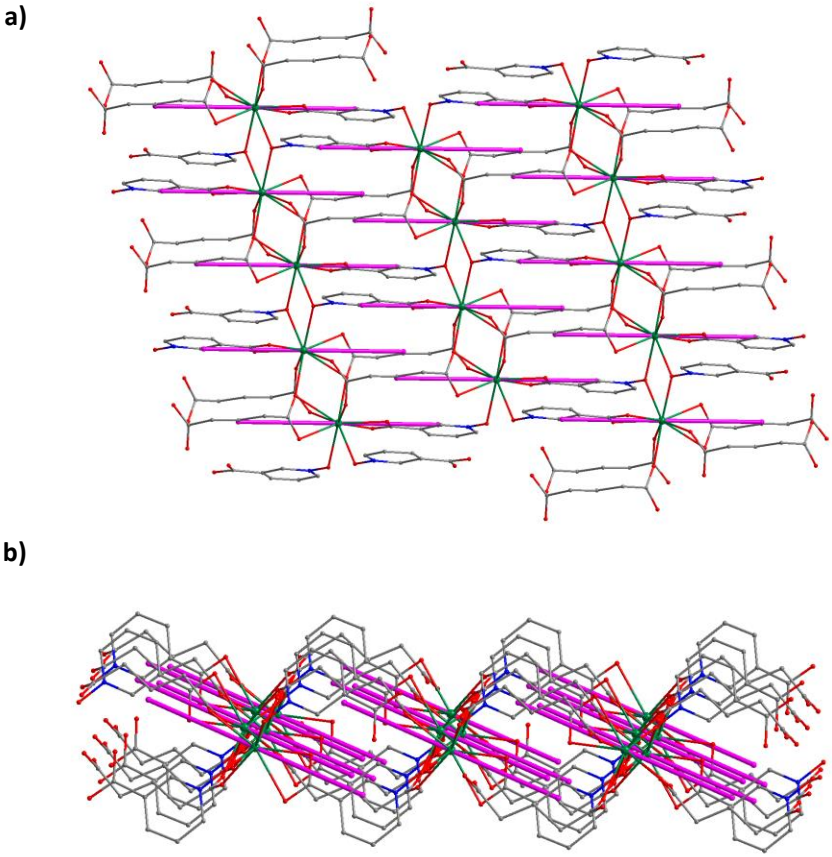

Fig. 6. Top(a) and side (b) view of magnetic axes (purple sticks) of the Dy^{3+} ions in the layer network of **3**.

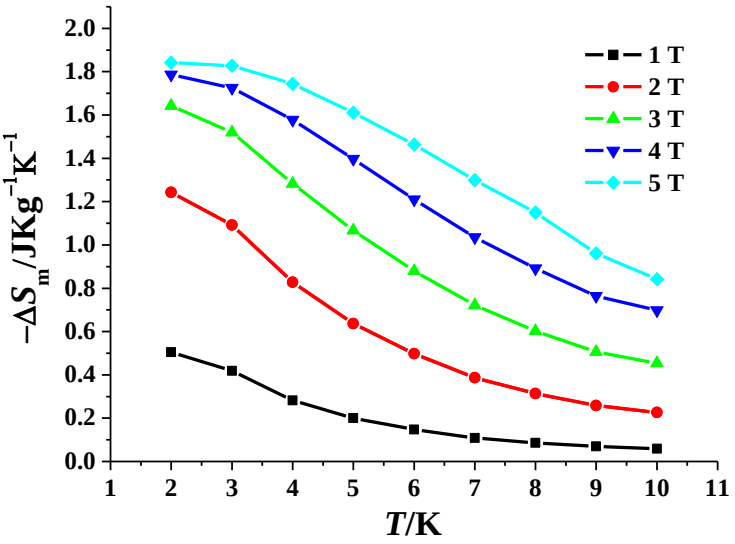

Fig. 7. Magnetic entropy change ($-\Delta S_m$) versus T of **2** for applied field changes ΔH.

Graphical Abstract

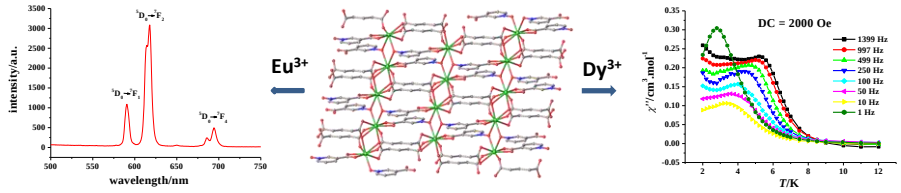

The isostructural 2D lanthanide coordination polymers may exhibit either luminescence or slow magnetic relaxation, depending on the lanthanide ions.